Journal of Fluorescence, Vol. 8, No. 2, 1998

Pressure Effects on Submicrosecond Phospholipid Dynamics Using a Long-Lived Fluorescence Probe

Piotr Targowski[1,2] and Lesley Davenport[1,3]

Received October 27, 1997; accepted February 27, 1998

The effects of applied external hydrostatic pressure on submicrosecond lipid motions in DPPC[4] bilayers have been examined using coronene (a long-lived planar fluorescent molecule) and DPH. Steady-state fluorescence emission anisotropy (EA) values ($\langle r \rangle$) obtained for probe-labeled DPPC SUVs measured at different fixed temperatures above T_c as a function of increasing hydrostatic pressure reveal pressure-induced lipid phase transition profiles. For coronene-labeled samples, the observed lipid "melt" profiles are broad and shifted to higher midpoint EA pressure values ($P_{1/2}$) compared with corresponding DPH-labeled SUVs at the same temperature. The data suggest lipid motions occurring on the submicrosecond time scale, detected only by using a long-lived fluorescence probe, which occur well above the normally reported "fluid–gel" lipid phase transition. Slopes of the pressure-to-temperature equivalence plots ($dP_{1/2}/dT$ = 39 bar/K) obtained for DPH- or coronene-labeled DPPC SUVs are identical within experimental error and reflect probe independence. For DPH, the slope of the $P_{1/2}(T)$ plot provides the expected phase transition phospholipid volume change. However, intercept values (at $P_{1/2}$ = 1 bar) or apparent phase transition temperatures obtained from the equivalence plots for the two probes are not equal. Differences appear to arise due to the very disparate fluorescence lifetime values of the two probes, which result in rotational sensitivity of coronene to gel lipid volume fluctuations occurring during the extended time window provided by coronene fluorescence.

KEY WORDS: Submicrosecond phospholipid dynamics; long-lived fluorescence emission anisotropy probe; hydrostatic pressure.

INTRODUCTION

High-pressure biophysics has emerged as an active research area in recent years for studying a wide range of biological macromolecular systems including protein conformation [1–4] and membrane lipid dynamics [5–8]. Hydrostatic pressure serves as an additional independent thermodynamic variable. Unlike temperature studies, effects arising from applied hydrostatic pressure arise solely from volume changes and, as such, are not "contaminated" by any associated thermal effects.

Although the fundamental physicochemical basis for pressure-induced effects are well established, the scale of these effects and their importance for biological

[1] Department of Chemistry, Brooklyn College of the City University of New York, 2900 Bedford Avenue, Brooklyn, New York 11210.

[2] Permanent address: Institute of Physics, Nicholas Copernicus University, ul. Grudziadzka 5, 87-100 Torun, Poland. Fax: 48-56-25397. e-mail: ptarg@phys.uni.torun.pl

[3] To whom correspondence should be addressed. Fax: 718-951-4827. e-mail: ldvnport@brooklyn.cuny.edu

[4] Abbreviations used: DPH, 1,6-diphenyl-1,3,5-hexatriene; DPPC, L-α-dipalmitoylphosphatidylcholine; DSC, differential scanning calorimetry; EA, fluorescence emission anisotropy; HEPES, *N*-2-hydroxyethylpiperazine-*N*′-2-ethanesulfonic acid; $K_p^{g/f}$, gel–fluid partition coefficient; P_m, lipid phase transition pressure; $P_{1/2}$, emission anisotropy midpoint pressure; SUVs, small unilamellar vesicles; T_c, lipid phase transition temperature at atmospheric pressure; THF, tetrahydrofuran.

1053-0509/98/0600-0121$15.00/0

systems are comparatively poorly defined. In particular, the effects of applied pressure on the *dynamic* "gel–fluid" heterogeneity of the lipid bilayer matrix has not been explored in any great detail. Most previous lipid membrane studies employing fluorescence and hydrostatic pressure effects have focused on the study of gel–fluid lipid domains, whereas the dynamics of this structural heterogeneity has been little explored and restricted primarily to investigations utilizing shorter-lived ($\langle\tau_{FL}\rangle$ < 100 ns) fluorescence probes [5,6]. However, more recent lipid dynamic studies, using pyrene derivatives [7] or parinaric acid [8], have demonstrated the applicability of longer-lived fluorescence probes to the dynamics of gel–fluid heterogeneous lipid systems.

In this study, the effects of applied hydrostatic pressure (0 to 1.2 kbar) on submicrosecond lipid dynamics within bilayer membranes have been examined using coronene, a long-lived (τ_{av} ~ 219 ns at 29°C in gel lipid) planar (D_{6h} symmetry) fluorescence probe. Previously we showed from thermal investigations [9] that depolarization of the fluorescence emission for coronene arises exclusively from "slow" *out-of-plane* rotations only ($\langle r\rangle_{op}$) and, combined with the long fluorescence lifetime measured in bilayer systems, makes this apolar membrane probe sensitive to submicrosecond dynamics of lipid chain disordering events which are occurring well after the decay of most other fluorescence probes commonly used for dynamic membrane studies such as 1,6-diphenyl-1,3,5-hexatriene (DPH)[4] ($\langle\tau_{FL}\rangle$ ~ 10.1 ns) [10]. In addition, we have shown that time-dependent EA profiles for coronene in lipid vesicle systems can be modeled and analyzed to provide quantitative estimates of submicrosecond gel–fluid fluctuation rates (k_{FG}). Investigations of the effect of applied hydrostatic on coronene-embedded lipid bilayers, as discussed here, demonstrate further evidence of submicrosecond lipid dynamics and, in addition, can also provide valuable thermodynamic information regarding submicrosecond fluid–gel lipid volume fluctutations effects, which can be detected only on this extended time scale.

EXPERIMENTAL

Materials and Methods

1,6-Diphenyl-1,3,5-hexatriene (DPH) and HPLC-purified coronene were obtained from Molecular Probes, Inc. (Eugene, OR), and used as supplied. L-α-Dipalmitoylphosphatidylcholine (DPPC) was purchased from Sigma Chemical Company and used without further purification, as discussed elsewhere [9]. Stock solutions of DPH (1 m*M*) and coronene (2 m*M*) were prepared in tetrahydrofuran (THF) and stored at −20°C in the dark. Absolute ethanol (200 proof, dehydrated), the pressure transducing fluid, was purchased from Pharmco (Bayonne, NJ) and used as supplied.

DPPC small unilamellar vesicles (SUVs) were prepared by sonication at 50°C in 10 m*M* HEPES containing 5 m*M* KCl and 140 m*M* NaCl, pH 7.2, buffer, followed by ultracentrifugation, as described in detail previously [9]. Labeling of DPPC SUVs with DPH was achieved by direct solvent injection [11] from the DPH/THF stock solution, resulting in a probe-to-phospholipid molar labeling ratio of 1:500. Residual organic solvent was removed by evaporation using a gentle stream of nitrogen gas. SUVs were incubated for at least 2 h at 50°C, with gentle swirling, to allow maximum absorption of the dye into the membrane. Coronene-labeled DPPC SUVs (probe-to-phospholipid molar labeling ratio of 1:200) were prepared by cosonication of the dye with lipid during vesicle preparation [12]. Unlabeled blank vesicle samples were matched by phosphorus concentration [13]. Typical phospholipid concentrations used for fluorescence measurements were ca. 0.2 m*M*. Under these conditions, the total absorption of the samples (arising from a combination of signals from both the dye absorption and the vesicle scatter) at the wavelength of excitation never exceeded 0.1, which obviated potential inner filter effects.

Fluorescence Measurements

Steady-state fluorescence emission anisotropy values ($\langle r(p)\rangle$), measured as a function of applied hydrostatic pressure (0–1.2 kbar), were determined using a high-pressure spectroscopy cell (HPSC-3K) mounted in an SLM 8000 spectrofluorimeter, essentially as described previously by Paladini and Weber [14]. The fluorometer was operated in the "ratio" mode in order to eliminate potential xenon lamp intensity fluctuations. A long-stemmed quartz cylindrical bottle (total volume, ~1.2 ml) was filled with the appropriate fluorescently labeled DPPC SUVs and sealed using a Teflon stopper, ensuring that all air bubbles were eliminated. The sample was loaded into the stainless-steel HPSC, filled with 200-proof ethanol, which served as the pressure-transmitting fluid, sealed, and connected to the pressure transducing pump. Temperature control was achieved using a water-circulating thermostated jacket surrounding the HPSC. A thermistor probe was used to monitor directly the internal temperature of the ethanol.

Four polarized fluorescence emission intensity components (I_{VV}, I_{VH}, I_{HH}, and I_{HV}) were measured by

integrating the analog signal collected over a 5-s interval for five consecutive periods, using Glan Thompson polarizers manually oriented either vertically or horizontally in the excitation or emission paths. Excitation and emission wavelengths were 340 and 448 nm, respectively, for coronene and 355 and 430 nm, respectively, for DPH. Excitation and emission bandwidths were each typically 4 nm.

Correction for induced scrambling of the four measured polarization components due to birefrigent pressure effects on the quartz observation windows of the HPSC was achieved using an extension of the method essentially described by Paladini and Weber [14]. However, in the approach employed here, rather than performing a second experiment to determine the combined (excitation and emission) scrambling coefficient, [α(p)] from a highly polarized sample with an expected observed EA value close to its known limiting anisotropy value [e.g., DPH in glycerol (4 μM); expected $r_0 = 0.4$], the independent scrambling factors, $X(p)$ (for excitation) and $Y(p)$ (for emission), may be resolved and were measured *simultaneously* at the time of sample data collection. This "direct" approach has been described in detail elsewhere [15].

For each applied pressure studied, the total fluorescence intensity was also calculated from the sum of integrated (and corrected) polarized intensities [$S(p)$], to provide estimates of the effect of applied pressure on the fluorescence lifetime of the sample since $\langle\tau(p)\rangle$ is proportional to $S(p)$ [11].

RESULTS AND DISCUSSION

For fluorescence probes with lifetimes of several tens of nanoseconds, the experimental averaging regime is extended. Under such conditions the fluorescence lifetime of the probe is now of the order of the lifetime of the refractory gel lipid ($\langle\tau_{FL}\rangle \sim \langle\tau_{GEL}\rangle$), and submicrosecond gel–fluid lipid dynamics or fluctuations can be successfully targeted [9]:

$$G \underset{k_{GF}}{\overset{k_{FG}}{\rightleftarrows}} F \qquad (1)$$

where F and G define the average concentrations of fluid and gel lipid fractions of the bilayer, respectively, ($F + G = 1$) and k_{FG} and k_{GF} represent the associated "gel–fluid" and "fluid–gel" exchange rates, respectively. At temperatures higher than the lipid phase transition ($T > T_c$), $G \rightarrow 0$ and $F \rightarrow 1$. For this simple compartmental model, the equilibrium distribution of gel and fluid lipid is expected to shift in response to temperature, applied pressure, and the presence of intrinsic (e.g., cholesterol and proteins) and/or extrinsic (e.g., Ca^{2+}) membrane modulators.

Steady-state fluorescence emission anisotropy (EA) values ($\langle r_{corr}\rangle$) for DPH- and coronene-labeled DPPC SUVs were determined as a function of increasing applied hydrostatic pressure (Figs. 1A and B, respectively) at four different but fixed temperatures above the phospholipid phase transition temperature (T_c = 39°C) [17]. As expected, at atmospheric pressure (p = 1 bar), where the lipid exists in the fluid phase, both lipid-embedded probes exhibit low EA values. However, with increasing applied hydrostatic pressure, a lipid-to-gel phase transition is observed, as reflected by increased measured EA values for the lipid-embedded fluorescence probes. EA values in the gel phase tend toward each probe's expected limiting anisotropy value [r_0(DPH) = 0.4 and r_0(coronene) = 0.1], reflecting increased restricted rotational motions for the probes when in the gel phase lipid. A modest increase (~20%) in corrected fluorescence intensity [$S(p)$] was also observed with increasing applied pressure for lipid embedded probes (data not shown), suggestive of a decreased rate of quenching by dissolved bilayer oxygen [18,19]. In addition, no significant spectral sensitivity was observed for coronene embedded in gel or fluid lipid regions, in contrast to the subtle environment sensitivity of the vibronic spectrum previously noted for DPH [5,20].

From the lipid "melt" profiles, the EA midpoint of the observed transition (denoted $P_{1/2}$) varies as a function of sample temperature. For coronene-labeled DPPC SUVs, pressure-induced lipid phase transitions (Fig. 1A) appear broad and much less well defined. However, it is clear that these profiles are shifted to higher $P_{1/2}$ pressure values compared with the more typical fluid–gel lipid transition profiles measured for DPH-labeled samples at the corresponding temperature (Fig. 1B). For example, at 44°C, $P_{1/2}$ = 0.72 kbar for coronene-labeled DPPC SUVs compared with the corresponding DPH-labeled sample, where $P_{1/2}$ = 0.1 kbar (Fig. 1C). In order to determine the $P_{1/2}$ values for the coronene-labeled SUVs, a value for the EA was chosen (equal to 0.045) as one-half of the maximum EA value achieved at a high applied hydrostatic pressure (p = 1.6 kbar) for all coronene samples studied. The exact value for this maximum EA has no physical relevance. The uncertainty of the $P_{1/2}$ values determined by this method are indicated by the error bars shown in Fig. 2. Our previous thermal studies of coronene-labeled DPPC SUVs [9] revealed similar

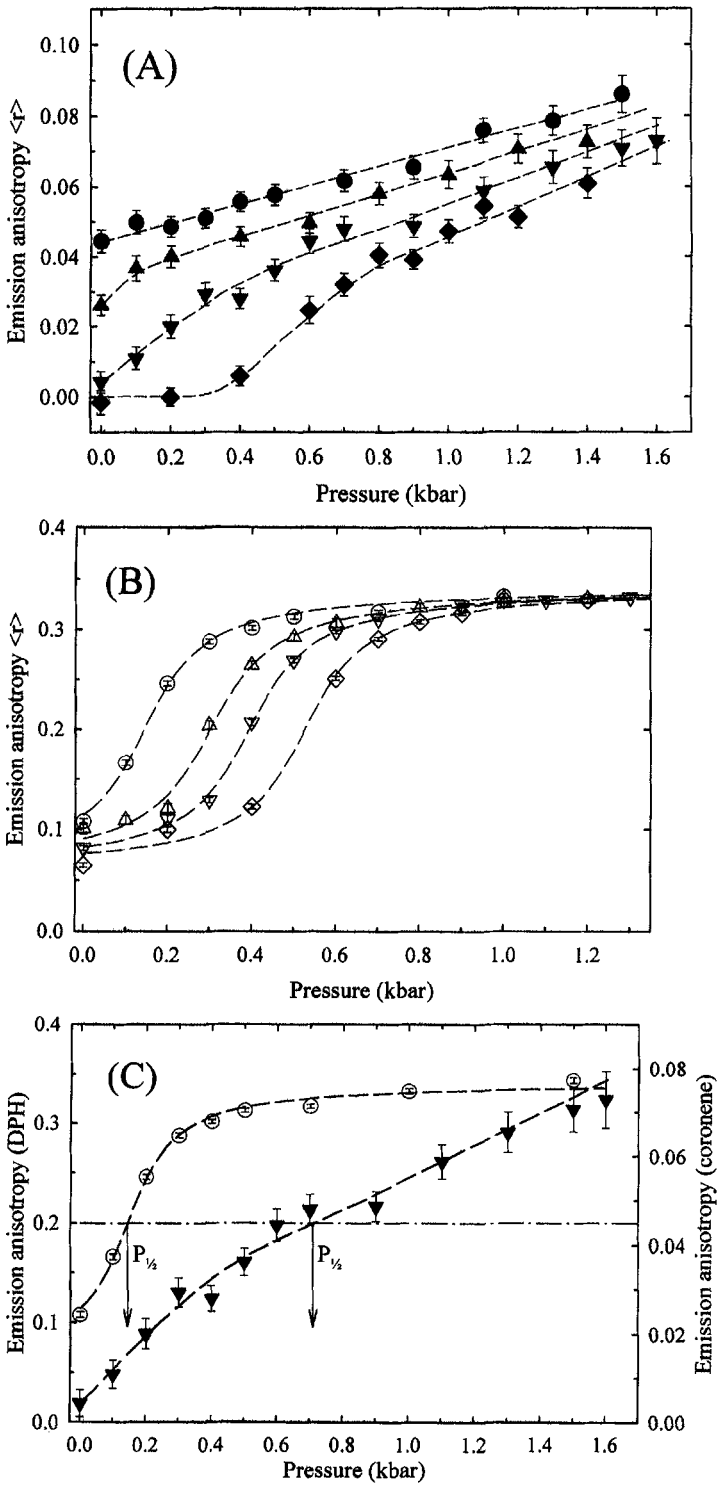

Fig. 1. Steady-state emission anisotropy as a function of increasing hydrostatic pressure $\langle r(p) \rangle$ for (A) coronene and (B) DPH-labeled DPPC SUVs at the following temperatures: for coronene, (● — ●)T = 26°C, (▲ — ▲)T = 35.8°C, (▼ — ▼)T = 43.6°C, and (◆ — ◆)T = 53.2°C; and for DPH, (○ — ○)T = 43.5°C, (△ — △)T = 47.3°C, (▽ — ▽)T = 50.3°C, and (◇ — ◇)T = 53.2°C. (C) shows the midpoint of the transition ($P_{1/2}$) for DPH- and coronene-labeled DPPC SUVs at 43.5°C. Values were corrected for scatter or birefrigency artifacts as discussed in the text. The probe-to-phospholipid molar labeling ratio used was 1:200 and 1:500 for coronene and DPH, respectively. Excitation was achieved at 340 and 355 nm, respectively, and the wavelengths of observation were 448 and 430 nm, respectively. Excitation and emission bandwidths were each typically 4 nm. Calculated errors were not greater than 0.005.

broad and shifted apparent lipid "melt" profiles and are characteristic for long-lived fluorescence probes [21]. Rather than preferential partitioning (K_{p}^{f} = 1 for coronene [9]) or lipid perturbation effects arising from the probe, these signatory "melt" profiles observed for long-lived fluorophores (e.g., pyrene [21]) may be inter-

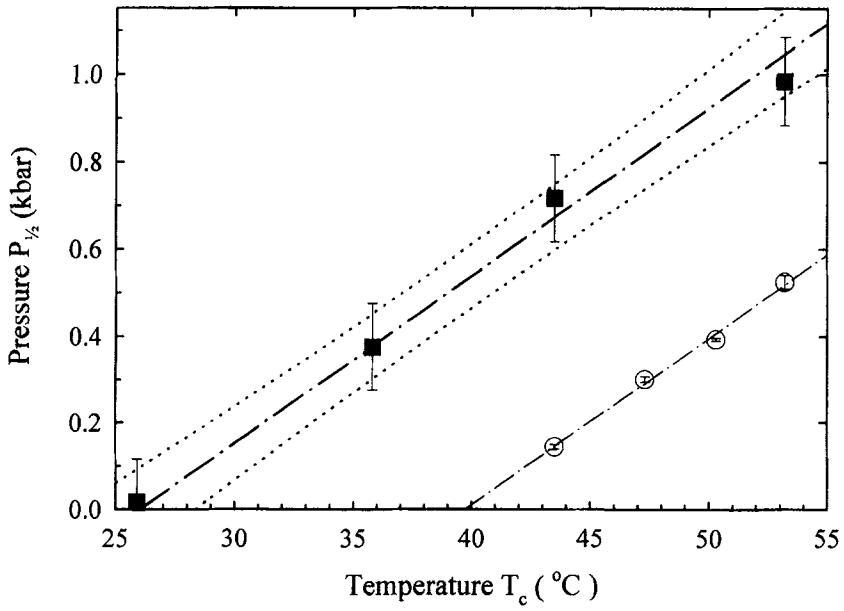

Fig. 2. Pressure-to-temperature equivalence plot for coronene (■ — ■)- and DPH (○ — ○)-labeled DPPC SUVs. Values of $P_{1/2}$ were determined from the midpoints of the lipid "melt" profiles shown in Fig. 1. For coronene data, the fit of the slope obtained for the DPH data are superimposed and shown with 95% confidence intervals.

preted as evidence for submicrosecond lipid dynamics and volume fluctuations occurring within gel lipid at pressures well above (or temperatures well below) the expected gel–fluid transition, resulting in probe rotational depolarization effects. These "persistent" lipid dynamics are detected by virtue of the long average fluorescence lifetime of the probe, resulting in an extended time window for experimental averaging.

Observed shifts of lipid melt profiles to higher $P_{1/2}$ values suggest that an increased pressure is required to hinder "slow" (submicrosecond) lipid motions occurring well above the normally reported "gel–fluid" lipid phase transition, and not detected by rotational motions of the more popular dynamic membrane fluorescence probes. Indeed even at higher pressures ($p \sim 1.6$ kbar), measured EA values for coronene do not converge and level off as for DPH at $p > 1$ kbar, which suggests that coronene is not fully hindered within the surrounding gel lipid environment on the submicrosecond time scale. Such long-range thermodynamic fluctuations of lipid chain conformation are believed to be responsible for several biologically important processes including passive cation transport [23] and bilayer destabilization required for membrane fusion [24] (for a review, see Ref. 21).

As shown previously [5–7,25], plots of the phase transition pressure (P_m) versus the lipid temperature (T) provide a pressure-to-temperature equivalence value, dP_m/dT. Clearly for DPH-labeled DPPC SUVs a transition pressure (P_m) may be identified with $P_{1/2}$. This permits use of the Clausius–Clapeyron equation to estimate the phospholipid volume change (ΔV) that occurs during the fluid-to-gel phase transition:

$$\frac{dP_m}{dT} = \frac{\Delta H}{T_c\,\Delta V} \tag{2}$$

where ΔH is the enthalpy change or heat of transition, and T_c is the atmospheric lipid phase transition temperature. A plot of $P_{1/2}$ values versus temperature for DPH (Fig. 2; circles) reveals a linear dependence, with *slope* = 39 ± 2 bar/K. Assuming for DPH that $P_m = P_{1/2}$, and using an enthalpy value (ΔH) of 8.7 kcal/mol determined previously from differential scanning calorimetric studies [23,24], a volume change at atmospheric pressure of $\Delta V = 30 \pm 1.5$ cm³/mol may be calculated using Eq. (2) with $T_c = 39.5$°C at atmospheric pressure for DPPC SUVs [17]. This ΔV value compares favorably with previous volumetric studies of DPPC from the pressure dependence of DPH polarization [5] and intramolecular excimer formation of dipyrenylphosphatidylcholines [7]. As discussed previously by Sassarolli *et al.* [7], the intercept of the pressure-to-temperature equivalence plot (Fig. 2) at atmospheric pressure ($P_{1/2} = 1$ bar) is

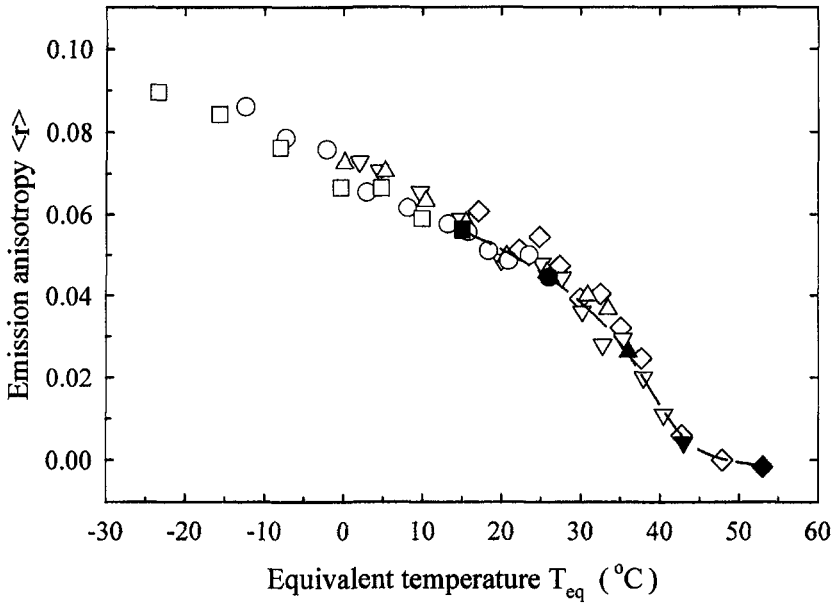

Fig. 3. Conversion of pressure data (from Fig. 1A) into equivalent temperature, $T_{eq}(T,p)$, according to Eq. (3), for coronene-labeled DPPC SUVs. Sample temperatures are (□)T = 15°C, (○)T = 26°C, (△)T = 35.8°C, (▽)T = 43.6°C, and (◇)T = 53.2°C. Data marked as respective solids are obtained at p = 1 bar, where T_{eq} = T. Consequently the connecting dashed line shows a corresponding thermal "melt" profile.

expected to correspond to the calorimetrically determined (and hence probe independent) lipid phase transition temperature (T_c). From extrapolation, the expected T_c value of 39.5°C is obtained for DPH-labeled DPPC SUVs [16].

For coronene-labeled DPPC SUVs, a similar pressure-to-temperature equivalence plot ($P_{1/2}$ versus temperature) (Fig. 2; squares) reveals (within experimental error) the same slope of 39 bar/K as for DPH. However, the apparent value for T_c at $P_{1/2}$ = 1 bar as estimated from the intercept value on the temperature axis of the pressure-to-temperature plot is found to be 26°C. While anomalous T_c values can reflect probe-induced bilayer perturbation effects, our previous studies [9] using coronene-labeled SUVS suggest that at the labeling ratios employed in these studies (not greater than 1:200 probe-to-phospholipid molar labeling ratio), this effect may be excluded. Rather, we believe, in analogy to our prior temperature-dependent studies, that the origins for the difference in extracted T_c values at $P_{1/2}$ = 1 bar, as reported from using short and long-lived fluorescence probes embedded within identical DPPC lipid vesicles, arise exclusively as a result of the long fluorescence lifetime for coronene. Indeed, the value of 26°C shows an excellent correspondence with values extracted from our previously measured temperature-dependent lipid phase transition profiles [9]. Thus "slow" lipid fluctuations occurring within gel lipid far before the major gel–fluid transition result in decreased EA values for long-lived probes. As a consequence, now $P_m \neq P_{1/2}$ and $T(P_{1/2}$ = 1 bar) $\neq T_c$.

Since $P_{1/2}(T)$ plots for DPPC SUVs labeled with either coronene or DPH demonstrate a linear relationship with the same slope, it is now possible to extend the pressure-to-temperature equivalence in a general way to describe *any* (p,T) conditions for this particular lipid which are probe independent. The equivalent temperature $T_{eq}(p,T)$ may be defined as

$$T_{eq}(T, p) = T - \frac{1}{\text{slope}} \cdot p \qquad (3)$$

where slope = 39 bar/K for DPPC SUVs.

Using Eq. (3), we can reexpress the pressure-dependent data shown in Fig. 1A for coronene in DPPC SUVs, as EA values versus the equivalent temperature, $T_{eq}(T,p)$ (Fig. 3). In principle, it is also possible to predict the pressure dependence of the "gel–fluid" exchange rate [$k_{FG}(p)$]. Assuming a simple two-state (G and F) compartmental model [Eq. (1)], we previously showed (Fig. 5A in Ref. 9) that atmospheric pressure values for the rotational correlation time, ϕ_{EFF} [where k_{FG} =

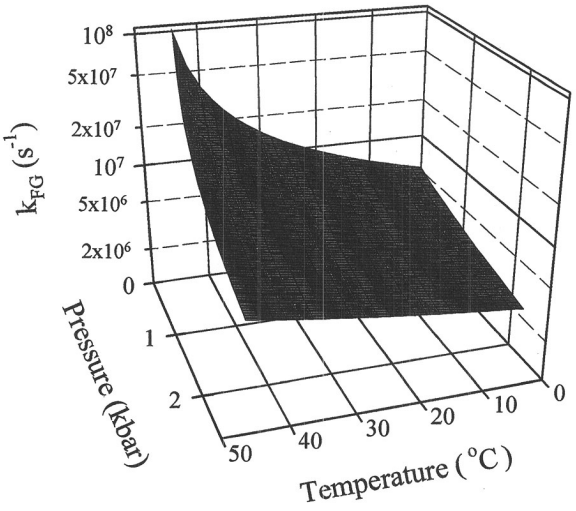

Fig. 4. Summary of the simulation showing the pressure and temperature dependence of the gel–fluid lipid exchange rate [$k_{FG}(p,T)$] for coronene-labeled DPPC SUVs. Values for k_{FG} at atmospheric pressure were previously determined from time-dependent EA studies of coronene/DPPC SUVs [9]. The pressure dependence was determined from Eq. (4), as discussed in the text.

$(\phi_{EFF})^{-1}$] determined from time-dependent EA studies revealed an empirical linear dependence on temperature, with slope $d\phi_{EFF}/dT = -4.1 \times 10^{-9}$ s/K. By adopting this simplification (in the absence of time-dependent pressure studies) the gel-to-fluid exchange rate (k_{FG}) at any applied hydrostatic pressure p may be reexpressed by the formula

$$k_{FG}^{-1}(T, p) = k_{FG}^{-1}(T, p = 1 \text{ bar}) + \delta \cdot p \qquad (4)$$

where for DPPC SUVs $\delta = 1.05 \times 10^{-10}$ s/bar. The results are summarized in Fig. 4. Clearly, submicrosecond lipid fluctuations are evident in gel lipid at applied hydrostatic pressures well above the main phase transition pressure (P_m) as normally reported by DPH. It is important to recognize that for the simple compartmental model assumed here, a discrete temperature- and pressure-dependent gel–fluid exchange rate is assumed. Alternate distributional analyses invoking a distribution of $k_{FG}(p,T)$ values [9] will require time-dependent pressure studies [28].

CONCLUSIONS

The aim of this study was to investigate the effects of applied hydrostatic pressure on DPPC SUV submicrosecond lipid dynamics. High-pressure fluorescence studies using short-lived bilayer probes such as DPH provide a static view of the structural lipid packing of the bilayer together with estimates of the phospholipid volume change (δV) occurring at the main gel–fluid lipid phase transition which compares favorably with those obtained in previous studies. However, for studies employing coronene, a long-lived fluorescence bilayer probe, insights into *submicrosecond* gel–fluid lipid fluctuations, preceding the main transition, are possible. These fluctuations may play a vital role in the regulation of important membrane-mediated events. In addition, consistent "slope" values ($dP_{1/2}/dT$) obtained from the pressure-to-temperature plots for both short- and long-lived probes suggest lipid dependence and probe independence and permit estimates of pressure-dependent gel–fluid rate constants [$k_{FG}(p)$] from prior thermal studies using coronene. Future studies are focused on quantitation of fluid–gel exchange rates and volume fluctuations using time-resolved fluorescence approaches [28].

ACKNOWLEDGMENTS

We thank Bo Shen for assistance with sample preparations. We express gratitude to Dr. Jay R. Knutson for use of the SLM HPSC-3K high-pressure spectroscopy cell used in these studies. We are grateful to Dr. Jay Knutson for helpful and insightful discussions. We acknowledge the assistance of Ms. Hazel Ward in the preparation of the manuscript. Research was supported in part by the National Science Foundation (Award DMB-9006044) and the American Heart Association. P.T. gratefully acknowledges additional support from the Polish Government through KBN Grant 2 PO3B 124 09. L.D. was an Investigator of the American Heart Association, New York City Affiliate.

REFERENCES

1. A. W. M. Rietveld and S. T. Ferreira (1996) *Biochemistry* **35**, 7743–7751.
2. S. Dallet and M.-D. Legoy (1996) *Biochim. Biophys. Acta* **1294**, 15–24.
3. J. L. Silva (1993) *Annu. Rev. Phys. Chem.* **44**, 89–113.
4. L. Erijman, A. A. Paladini, G. H. Lorimer, and G. Weber (1993) *J. Biol. Chem.* **268**, 25914–25919.
5. P. L.-G. Chong and G. Weber (1983) *Biochemistry* **22**, 5544–5550.
6. P. L.-G. Chong, B. W. van der Meer, and T. E. Thompson (1985) *Biochim. Biophys. Acta* **813**, 253–265.
7. M. Sassaroli, M. Vauhkonen, P. Somerharju, and S. Scarlata (1993) *Biophys. J.* **64**, 137–149.
8. C. R. Mateo, P. Tauc, and J.-C. Brochon, (1993) *Biophys. J.* **65**, 2248–2260.
9. L. Davenport and P. Targowski (1996) *Biophys. J.* **71**, 1837–1852.

10. L. Davenport, J. R. Knutson, and L. Brand (1986) *Biochemistry* **25**, 1811–1816.
11. L. A. Chen, R. E. Dale, S. Roth, and L. Brand (1977) *J. Biol. Chem.* **252**, 7500–7510.
12. L. Davenport (1997) in L. Brand and M. L. Johnson (Eds), *Methods in Enzymology, Vol. 278*, Academic Press, New York, pp. 487–512.
13. C. W. F. McClare (1971) *Anal. Biochem.* **39**, 527–530.
14. A. A. Paladini and G. Weber (1981) *Rev. Sci. Instrum.* **52**, 419–429.
15. P. Targowski and L. Davenport (1998) *Analytical Biochemistry*, submitted for publication.
16. R. F. Chen and R. L. Bowman (1963) *Science* **147**, 729–732.
17. B. R. Lentz, Y. Barenholz, and T. E. Thompson (1976) *Biochemistry* **15**, 4529–4537.
18. S. Fischkoff and J. M. Vanderkooi (1975) *J. Gen. Physiol.* **65**, 663–676.
19. A. K. Tan and R. Ramsey (1993) *Biochemistry* **32**, 2137–2143.
20. L. Davenport, J. R. Knutson, and L. Brand, (1986) *Biochemistry* **25**, 1811–1816.
21. L. Davenport and P. Targowski (1995) *J. Fluoresc.* **5**, 9–18.
22. L. Davenport, J. Z. Wang, and J. R. Knutson (1989) in A. Butterfield (Ed.), *Biological and Synthetic Membranes*, Alan R. Liss, New York, pp. 97–106.
23. J. F. Nagle and J. L. Scott, Jr. (1978) *Biochim. Biophys. Acta* **513**, 236–243.
24. D. Hoekstra (1982) *Biochemistry* **21**, 2833–2840.
25. N.-I. Liu and R. L. Kay (1977) *Biochemistry* **16**, 3484–3486.
26. S. Mabrey and J. M. Sturtevant (1976) *Proc. Natl. Acad. Sci. USA* **73**, 3862–3866.
27. B. DeKruiff, R. A. Demel, A. J. Slotboom, L. L. M. VanDeenen, and A. F. Rosenthal (1973) *Biochim. Biophys. Acta* **307**, 1–19.
28. L. Davenport, P. Targowski, and J. R. Knutson (1995) *Biophys. J.* **68**, A303.